PROCEEDINGS, 51st Workshop on Geothermal Reservoir Engineering
Stanford University, Stanford, California, February 9-11, 2026
SGP-TR-230

Evaluation of Proppant Performance in Maintaining Fracture Conductivity Under Simulated Geothermal Reservoir Conditions

Najiba Hozeh, Wahidur Rahaman, Xuejun Zhou, Sree Sujon Sutradhor, Ahmad Ghassemi

Reservoir Geomechanics and Seismicity Research Group, The University of Oklahoma, Norman, OK, USA

Ahmad.ghassemi@ou.edu

Keywords: crush resistance, flow-through experiments, fracture conductivity, proppant, proppant-pack

ABSTRACT

The long-term effectiveness of hydraulic fracturing in geothermal and unconventional reservoirs critically depends on the ability of proppants to maintain open flow pathways under in-situ stress and temperature. This study presents a laboratory-based evaluation of proppant performance using a series of flow-through experiments designed to replicate reservoir-relevant conditions, including elevated confining pressures, high temperatures (up to 250 °C), and continuous fluid flow. Fracture conductivity is commonly used as the key parameter traditionally used in field-scale fracture design, so we report it as the primary measurable indicator of how proppants contribute to maintaining fracture conductivity over extended periods of loading. A suite of proppant-packed fracture analogs was constructed and tested to characterize their mechanical and thermal responses during progressive loading. The experiments captured how fracture conductivity evolves as a function of proppant type (resin coated, low density ceramic, pet coke, & Sand), grain strength, thermal stability, and interactions with the surrounding rock or bounding surfaces. Results show that conductivity degradation varies significantly among proppants: some materials retain permeability even under severe thermo-mechanical conditions, whereas others exhibit substantial loss due to embedment, compaction, thermal softening, or grain crushing. The results contribute to improving proppant selection and fracture-design strategies for high-stress, high-temperature reservoirs, where long-term fracture performance is essential for sustained production.

1. INTRODUCTION

Multistage hydraulic fracturing is being used in geothermal reservoir development. A major concern in hydraulic fracturing is the retention of fracture permeability at the end of pumping providing impetus for the use of proppants to keep the fracture open. In petroleum applications, a variety of natural and manufactured materials have been used for this purpose. Depending on the expected magnitude of the closure stress, sand or ceramic particles—are placed within fractures to resist in-situ stresses and enhance fracture conductivity by preventing fracture closure. Their selection and proper evaluation are critical, as proppant properties strongly influence the success of hydraulic fracturing treatments. In practical field applications, factors such as proppant cost, density, and mechanical strength must be carefully considered because large quantities of proppant are mixed with water and injected into the formation ((Mittal et al., 2017; Zheng et al., 2018; Sutradhor and Ghassemi, 2025). A propped fracture is considered successful when it can maintain conductivity during production, even as various external forces act to reduce its width and permeability (Kurz et al., 2013). Numerous studies have examined the factors that influence fracture conductivity. Early work (e.g., Cooke, 1973). demonstrated that fracture conductivity decreases with increasing temperature and pressure. Nguyen et al. (2018) later showed that proppant breakage, particle embedment, and migration of fines all contribute to conductivity loss. Proppant particle size was also shown to affect conductivity (Shah, 2010). Collectively, these studies highlight the complex behavior of propped fractures under varying thermo-mechanical conditions. However, these investigations have been limited to relatively low temperature conditions.

In this work, we present the laboratory testing results for evaluating proppant performance in maintaining fracture conductivity under geothermal reservoir conditions of high temperature up to 250 °C and high stress up to 70 MPa. These elevated temperature and pressure conditions allow us to mimic the harsh environments encountered in deep, high-temperature geothermal and unconventional reservoirs. The results from this study can assist engineers in optimizing hydraulic fracturing designs and improving production from tight formations worldwide. Several commercially available proppants were examined, including resin-coated ceramics, petroleum coke (pet-coke), and low-density ceramics (Ko and Ghassemi, 2023; Sutradhor and Ghassemi, 2025). The ability of these materials to maintain fracture conductivity under extreme temperature and stress conditions has direct implications for the durability of stimulation treatments, long-term fracture stability, and the efficiency of geothermal heat extraction.

2. EXPERIMENTAL SETUP

In this study we used a purpose-built steel frame to contain the proppant bed for flow-through testing. The frame follows the same general principle as the stacked-shim cell (a defined cavity bounded by rigid pistons), but its external geometry and mounting features were adapted to fit our laboratory requirements and instrumentation. The frame is designed to be clamped between the platens of a hydraulic load frame (e.g., MTS-816 series) and can be fitted with standard ports for inlet/outlet flow, thermocouple ports.

The proppant bed, typically 0.3–0.5 cm thick (concentration 1 lb/ft^2), was carefully placed to ensure uniform contact with the opposing rock surfaces. The rock used is Sierra White granite, often used for geothermal related laboratory research(Ye & Ghassemi, 2018). Fluid flow was directed along the long axis of the proppant bed to simulate realistic in-situ flow paths, while axial stress was applied to the granite assembly to replicate the overburden pressure present in the reservoir. The embedded configuration allows simultaneous

monitoring of permeability and fracture deformation, and a heating pack surrounding the steel frame maintained the temperature at the desired set point. Temperature and stress were regulated and recorded to reproduce high-temperature, high-pressure reservoir conditions, providing a controlled environment for assessing proppant performance under realistic operational scenarios. This setup ensures that the experimental results capture the coupled effects of mechanical loading, thermal exposure, and fluid flow on fracture conductivity. Figure 1 illustrates the proppant pack embedded between the two granite blocks, highlighting the configuration used in the flow-through experiments. At this stage of our work, smooth granite surfaces were used to ensure uniform contact with the proppant bed and to minimize surface irregularities that could influence flow paths.

Figure 1. Proppant pack embedded between two Sierra White granite blocks, showing the experimental configuration used in flow-through tests.

For a cuboid-shaped thin proppant bed, its permeability can be estimated directly using Darcy's law:

$$k = \frac{Q\,\mu\,L}{A\,\Delta P}$$

where:

- Q is the volumetric flow rate through the proppant bed,
- μ is the dynamic viscosity of the fluid, which depends on temperature,
- L is the flow path length along the bed,
- $A = w \cdot b$ is the cross-sectional area of flow, with b being the thickness of the proppant bed and $w$its width,
- ΔP is the pressure difference across the sample.

Fracture conductivity is then calculated as $C_f = k \cdot b$. The conductivity of the proppant bed depends on the boundary conditions. These conditions include mechanical boundary conditions (closure pressure), hydraulic boundary conditions (pressure differentials), geometric boundary conditions (dimensions and constraints of the specimen), and thermodynamic boundary conditions (temperature and fluid properties).

Under high-energy flow conditions—characterized by large pressure differentials—conductivity tends to be higher but less stable, potentially due to the activation of preferential flow pathways within the proppant pack. In addition, large pressure gradients may also temporarily enhance fracture conductivity through mechanisms such as proppant rearrangement, fines mobilization. However, these processes can also induce structural instability within the proppant pack, resulting in time-dependent and unstable conductivity. To approximate field-scale fluid pressure gradients (typically several hundred psi over 100 meters) in laboratory experiments, a scaled-down pressure difference of a few psi is applied across the sample, considering its dimensions. The resulting flow follows Darcy's law, and the calculated Reynolds numbers typically range from 0.0001 to 0.50 (<1), confirming laminar flow through the porous proppant medium.

3. PROPPANT SELECTION

Three distinct proppant materials were selected for these tests: petroleum coke–based proppants (PC), high-transported ultra-low-density ceramic proppants (LDC), and resin-coated ceramic proppants (RC) (Ko et al., 2023; Sutradhor and Ghassemi, 2025). These proppants represent a broad range of mechanical strengths, densities, and thermal stabilities, allowing evaluation of their performance across different reservoir environments (Table 1). PC proppants, derived from petroleum coke, are lightweight and economical but may be more susceptible to crushing at high stresses. LDC proppants are engineered for long-distance transport and placement efficiency, offering low density but moderate strength. In contrast, RC proppants incorporate a resin coating designed to improve fines control, enhance mechanical integrity, and reduce proppant flowback during production.

Table 1: Different properties of the proppants of various size

Proppant Type	Sizes	Bulk Density (gm/cm^3)	Proppant shape (X=Roundness, Y=Sphericity)	Packing strength (psi)	K-value	Fine generates at K-value (%)
PC	10_35	1.09	(0.7, 0.7)	2100	2K	6.67
LDC	10_35	1.21	(0.9, 0.9)	3600	4K	7.77
RC	10_35	1.60	(0.9, 0.9)	10,200	15K	7.50
Sand	10_35	1.521	(0.5,0.6)	910	1K	4.23

Earlier laboratory studies typically focused on packing strength or mechanical resistance under confined loading, often without incorporating fluid flow or temperature effects. In this study, however, the proppant performance is assessed under a more realistic combination of conditions, integrating mechanical stress, elevated temperature, and fluid flow to evaluate fracture conductivity. This approach provides a more comprehensive assessment of each proppant's ability to maintain permeability over time and sustain effective fluid flow under field-representative geothermal and unconventional reservoir conditions.

Scanning Electron Microscopy (SEM) is used to observe fine surface textures, detect potential defects, and assess material integrity at the micrometer to nanometer scale. SEM was used to capture the intact surface morphology of three proppant types—petroleum coke (PC), low-density ceramic (LDC), and resin-coated ceramic (RC)—prior to exposure to high pressure and high temperature conditions (Figure 2). The SEM images reveal that the surfaces of all three proppants are smooth and structurally uniform, with no observable microcracks, particle breakage, coating delamination, or other visible defects. The absence of pre-existing damage is important, as it establishes a clear baseline for evaluating the mechanical and thermal degradation that may occur during subsequent loading experiments. By confirming that each proppant type began the tests in a defect-free state, the post-experiment SEM results can be accurately interpreted to isolate changes caused solely by the imposed stress and temperature conditions.

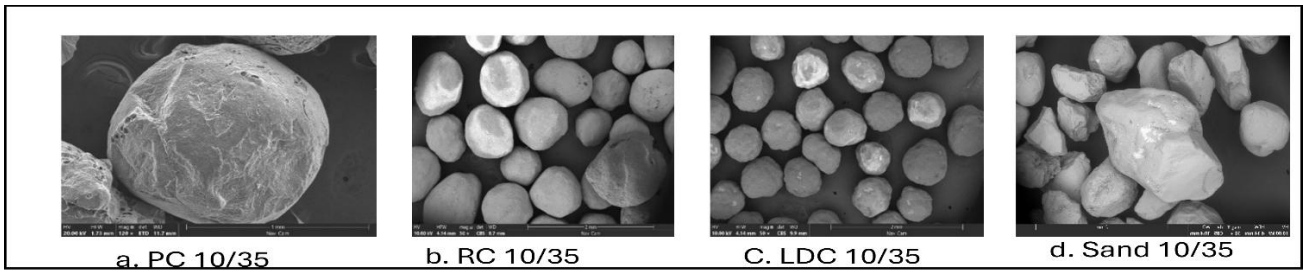

Figure 2. High-magnification (50×) SEM images showing the surface morphology of the petroleum coke (PC), low-density ceramic (LDC), resin-coated ceramic (RC) proppants and sand 10/35 prior to testing.

Proppant packs were embedded within smooth, polished granite fracture surfaces, prepared in a rectangular geometry to ensure well-defined flow pathways and reproducible testing conditions. The use of a highly smooth fracture at this stage allowed for isolating the fundamental hydraulic behavior of the proppants without the added complexity introduced by natural fracture roughness. In constructing each specimen, careful attention was given to achieving an even distribution of the proppant grains across the fracture plane. This minimized localized bridging or void formation and supported uniform fracture width along the flow direction. Such consistency is essential for accurately assessing fracture conductivity and for comparing the mechanical and thermal responses of different proppant types under controlled laboratory loading and temperature conditions.

Table 2: Dimension of the rock samples and proppant bed used in the experiment

Sample ID	Proppant type	Proppant bed thickness (mm)	Proppant bed weight (g)	Host rock thickness(mm)	
				Top section	Bottom section
ReA	LDC (10_35)	4.0	37.0	30.3	28.5
ReB	RC (10_35)	3.3	39.0	30.3	28.5
ReC	PC (10_35)	4.5	37.0	35.5	31.0
ReE	Sand(10_35)	3.3	37.0	33.8	34.0

4.TEST PROCEDURE

Testing procedures can be divided into two major components: pressure variation and temperature variation. To accurately evaluate how fracture conductivity responds to changes in pressure and temperature, it is essential that boundary conditions are carefully controlled. Only one variable—either pressure or temperature—should be adjusted at a time, while all other factors (axial load, confining pressure, flow rate, temperature, or pressure differential) remain constant. Without this control, the individual influence of each parameter would be difficult to isolate, and the resulting conductivity behavior would be ambiguous.

In the pressure-variation stage, mechanical loading is systematically increased to understand how proppant-supported fractures respond to increasing axial stresses. Once the mechanical influence is fully characterized, the test transitions into the temperature-variation stage, where temperature is changed stepwise under fixed mechanical conditions to determine how thermal effects alter flow capacity. This two-stage design ensures that the mechanical and thermal contributions to conductivity evolution are evaluated independently, allowing a clearer interpretation of proppant performance under reservoir-representative conditions.

The experimental workflow for cuboid proppant-bed samples consists of three sequential stages designed to isolate the effects of mechanical loading and temperature on fracture conductivity. The goal is to distinguish how conductivity evolves under (a) axial stress, (b) elevated temperature, and (c) mechanical crushing at the final loading stage.

5.TEST RESULTS

5.1 Sample ReA (LDC proppant):

During the conductivity tests performed with low-density ceramic (LDC) proppant, the axial load was cycled below 4000 psi while the temperature was raised to a maximum of 220 °C. At last stage, the axial load was ultimately increased up to 9,500 psi. Throughout the experiment, fluid overflow was collected at each temperature stage to document any changes in effluent appearance, and the proppant bed was inspected after exposure to combined high temperature and high stress. A noticeable change in the effluent color was observed as temperature increased: the initially clear flow gradually turned darker at elevated temperatures. This darkening suggests increasing dissolution, mobilization of fines, or thermal alteration of the proppant surface (Figure 3, left). Despite the darkening of the effluent at elevated temperatures, the proppant bed appeared generally intact at the macroscopic scale, with only limited or regionally distributed crushing visible after testing under the highest loads and temperatures (Figure 3, right). While significant deformation was not immediately apparent to the naked eye, localized grain breakage and subtle compaction were evident upon closer inspection. SEM analysis further confirms these observations, revealing micro-scale damage such as surface alteration, partial grain fusion, and localized crushing that is not easily detectable through visual examination alone (Figure 4). Together, these observations indicate that although the LDC proppant maintains an overall coherent structure under simulated deep-reservoir conditions, measurable mechanical and thermal degradation does occur at the grain scale, which may contribute to the observed reduction in fracture conductivity.

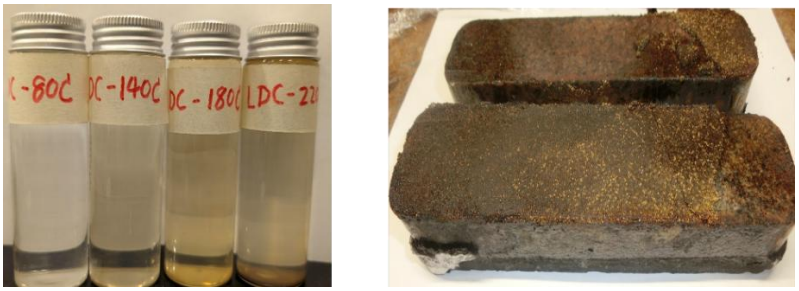

Figure 3: Left: Effluent collected at different temperature stages during LDC proppant testing, showing progressive darkening of the fluid with increasing temperature. Right: Post-test LDC proppant bed exposed to combined high temperature (up to 220 °C) and high axial stress (up to 9,500 psi), showing evidence of some particle crushing while still retaining overall structural integrity under extreme conditions.

Furthermore, the SEM images (Figure 4) reveal notable alterations in both surface texture and grain-to-grain interactions. Compositional contrast images show bright patches corresponding to foreign or thermally altered material attached to the proppant surfaces, while the darker regions represent the original ceramic matrix. Higher-magnification morphology images highlight significant surface roughening, micro-fracturing, and evidence of grain fusion. In several areas, adjacent proppant grains appear partially sintered or bonded together, likely due to exposure to extreme thermal and mechanical conditions. This fusion reduces pore space and disrupts the granular structure, helping to explain the observed loss of fracture conductivity during testing.

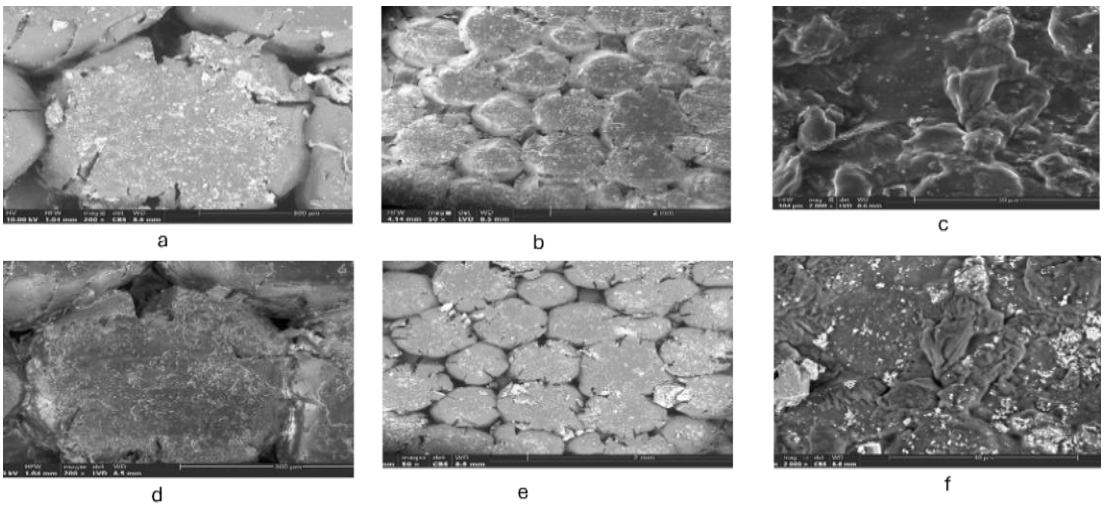

Figure 4: SEM representation of LDC at (a,d) 50× magnification, (b,e) at 200× magnification, (c,f) at 2000× magnification. Panels (a), (b), and (c) show compositional contrast, where bright regions indicate foreign or thermally altered material adhered to the proppant surface, while darker regions represent the original ceramic grains. Panels (d), (e), and (f) present detailed

surface morphology, revealing substantial microstructural alteration. Evidence of grain fusion is observed in several locations, likely caused by the combined effects of elevated temperature and mechanical loading. Such fusion reduces intergranular pore space, which can significantly diminish fracture conductivity.

Overall, fracture conductivity decreases with both temperature and axial stress. When heating under a constant axial stress of 1000 psi and a fixed pressure differential between the upstream and downstream pumps, a general decline in conductivity is observed as temperature increases (Figure 5, left). Under constant temperature conditions, fracture conductivity also decreases with increasing axial stress. Notably, once stress reduced, conductivity may not fully recover even after lowering the axial stress, suggesting possible irreversible deformation or rearrangement of the proppant (Figure 5, right).

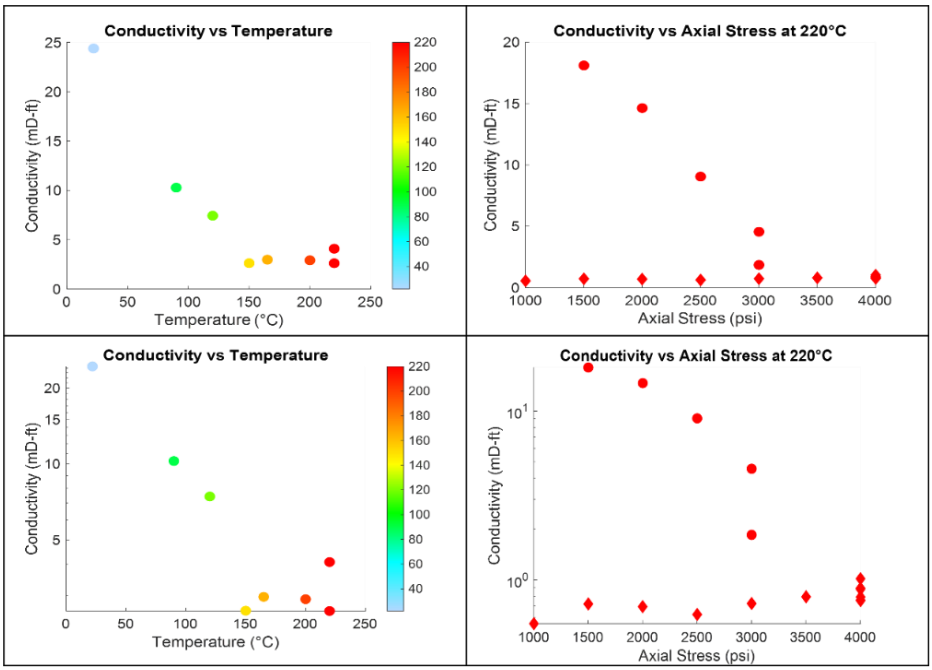

Figure 5. LDC proppant test results (Color denotes temperature, increasing from low (cool colors) to high (warm colors)). Left column: proppant pack conductivity as a function of temperature under a constant axial stress of 1000 psi and fixed pressure differential; Right column: proppant pack conductivity response to varying axial stress under constant temperature conditions of 220 °C, showing irreversibility after stress reduction. Upper row: Conductivity plotted on a linear y-axis. Lower row: Same data plotted on a logarithmic y-axis to highlight order-of-magnitude changes at low conductivity levels.

For LDC, conductivity trend remain consistent up to its packing strength of approximately 4000 psi, beyond which grain rearrangement and fines generation begin to contribute to additional flow restriction. At elevated temperatures, degradation of the cell sealing material occasionally introduced partial blockage in the flow path, leading to sharp conductivity drops near the end of some tests. However, these late-stage effects do not alter the overall observed trend, in which conductivity decreases systematically with increasing temperature and axial stress.

5.2 Sample ReB (RC proppant):

During conductivity testing of the high-strength resin-coated (RC) proppant, the axial load was cycled below 8,000 psi while the temperature was elevated to a maximum of 220 °C. Throughout the experiment, fluid effluent was collected at each temperature stage to monitor changes. A noticeable darkening of the effluent was observed as temperature increased, shifting from initially clear to a darker hue (Figure 6, left). This change suggests potential thermal degradation of the resin coating, mobilization of fines, or dissolution products.

Post-test inspection of the proppant pack under macroscopic examination revealed a generally intact structure, even after exposure to the highest stress and temperature (Figure 6, right). However, closer inspection indicated subtle signs of deformation, including localized pellet embedding and slight compaction, but no widespread crushing.

Figure 6: Left: Darkening of effluent fluid across temperature stages during RC proppant testing. Right: The overall intact proppant pack after exposure to final conditions of 10,000 psi and 220 °C.

Scanning Electron Microscope (SEM) analysis provided further detail, revealing micro-scale damage not visible to the naked eye. This included evidence of resin coating softening, grain coalescence, and localized coating delamination or peeling (Figure 7). These findings indicate that while the high-strength RC proppant pack maintained its macroscopic integrity under simulated deep-reservoir conditions, it experienced measurable thermo-mechanical degradation at the grain scale. This degradation, particularly the softening and deformation of the resin coating, is likely contributor to the observed reduction in long-term fracture conductivity.

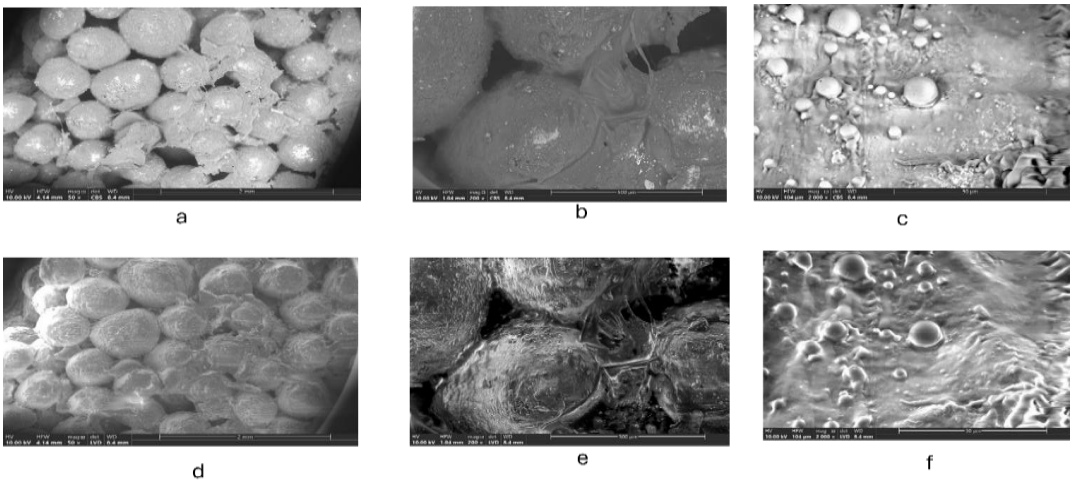

Figure 7. SEM analysis of resin-coated (RC) proppant after exposure to high temperature and stress. Images are presented at (a, d) 50×, (b, e) 200×, and (c, f) 2000× magnification. Panels (a), (b), and (c) show compositional contrast, where bright areas suggest the presence of debris or thermally degraded resin, contrasting with the darker underlying proppant substrate. Panels (d), (e), and (f) detail the surface morphology, revealing substantial microstructural alteration. Evidence of resin softening, plastic deformation, and grain coalescence is visible, a consequence of the combined high temperature and mechanical loading. This deformation reduces intergranular pore space and is a primary mechanism for the observed decline in fracture conductivity.

Fracture conductivity consistently decreases with both increasing temperature and axial stress. At 22 °C, conductivity declines rapidly as axial stress rises from ~600 psi to ~4000 psi, indicating progressive compaction and reduced flow capacity. At 100 °C, conductivity values are systematically lower than at 22 °C across all stress levels, showing that elevated temperature weakens the proppant pack's ability to maintain conductive pathways. At 200 °C, conductivity decreases even more sharply with stress, with very low values reached at higher loads, reflecting substantial loss of fracture openness under combined high stress and temperature. Overall, the results show a strong combined effect of temperature and axial stress on reducing fracture conductivity, with higher temperature accelerating the stress-induced loss of permeability (Figure 8).

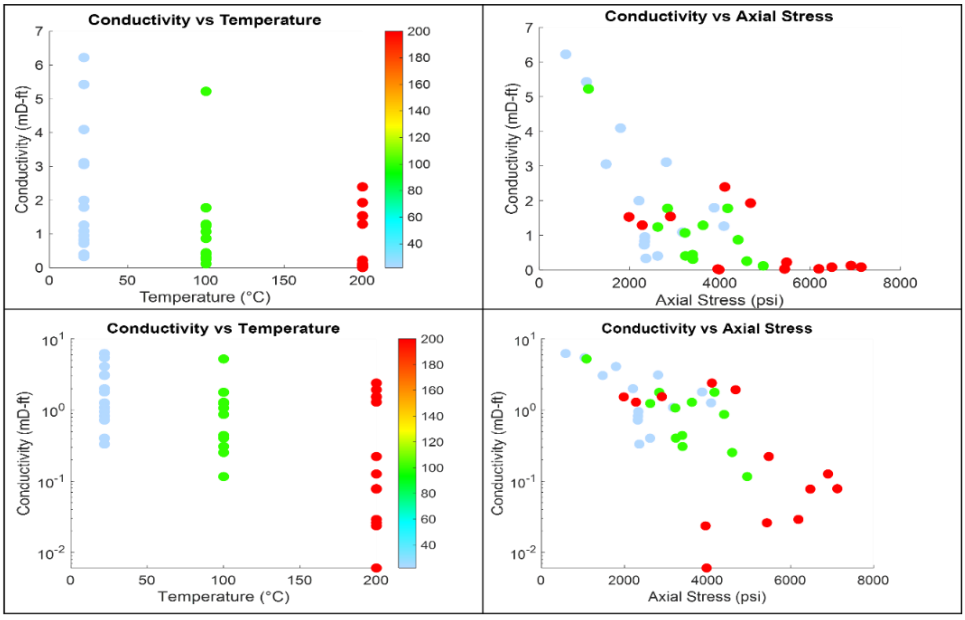

Figure 8. RC proppant test results (Color denotes temperature, increasing from low (cool colors) to high (warm colors)). Left column: Proppant pack conductivity as a function of temperature, showing progressive decline in conductivity as temperature increases from 22 °C to 200 °C under a gradual increase in axial stress up to 8000 psi.Right column: Conductivity response to axial stress at different temperature stages (22 °C, 100 °C, and 200 °C). Higher temperatures lead to more rapid conductivity loss with stress. Upper row: Conductivity plotted on a linear y-axis. Lower row: Same data plotted on a logarithmic y-axis to highlight order-of-magnitude changes at low conductivity levels.

RC tests were conducted up to an axial stress of approximately 8000 psi. A sharp decline in conductivity was observed beyond about 6000 psi, which is attributed to the onset of fines generation and partial blockage of the flow path, potentially exacerbated by high-temperature degradation of the sealing material. Despite this late-stage instability, the conductivity data at lower and intermediate stress levels remain consistent and clearly show a systematic decrease with increasing temperature and axial load, indicating that the overall trend is robust and not dominated by end-of-test artifacts.

5.3. Sample ReC (PC proppant):

The test was completed successfully, with all procedures executed according to the planned methodology. Post-test inspection showed that the proppant pack remained well consolidated, with no visible signs of significant particle displacement or channel development (Figure 9, right). Fluid overflow was collected at 22 °C, 100 °C, and 200 °C to document changes in effluent appearance with increasing temperature. At 200 °C, the overflow initially displayed a dark coloration that became clear after standing for one day, indicating a transient response rather than sustained deterioration. Thus, two bottles represent the 200 °C condition: an early-stage yellowish fluid and a later clear fluid. Despite this temporary discoloration at elevated temperature, the proppant bed maintained good macroscopic integrity throughout the test (Figure 9, left).

Figure 9: Left: Effluent fluid across temperature stages during PC proppant testing. Right: The overall intact proppant pack after exposure to final conditions of 5,000 psi (which exceeds crush resistance ~2100 psi of the PC) and 200 °C.

SEM analysis provides detailed insight into temperature- and stress-induced changes that are not readily detectable at the macroscopic scale. SEM images of PC 10/35 proppant were collected at multiple magnifications to capture both compositional contrast and surface morphology (Figure 10). Panels (A), (C), and (E) highlight contrast between the proppant grains and foreign or thermally affected material, where bright regions correspond to debris or altered resin and darker regions represent the underlying proppant. Panels (B), (D), and (F) illustrate the corresponding surface morphology, revealing pronounced microstructural alteration. Clear evidence of deep crack, severe surface roughening, plastic deformation, and material disintegration is observed, reflecting the combined influence of elevated temperature and mechanical loading. These microstructural changes reduce intergranular pore space and represent a key mechanism contributing to the observed decline in fracture conductivity.

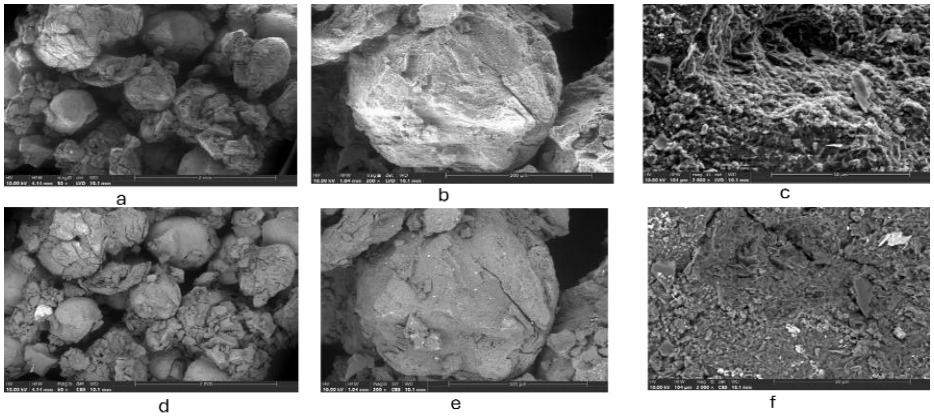

Figure 10. SEM micrographs of PC 10/35 proppant after combined thermal and mechanical loading. Panels (a–c) present compositional contrast at 50×, 200×, and 2000× magnification, highlighting bright regions associated with foreign material or thermally affected resin. Panels (d–f) show corresponding surface-morphology views, revealing pronounced microstructural modification. Features such as resin softening, localized plastic deformation, and partial grain coalescence are evident, indicating progressive alteration of grain contacts and narrowing of pore pathways under elevated temperature and stress.

Fracture conductivity shows a clear dependence on both temperature and axial stress (Figure 11). At lower temperatures, conductivity remains relatively high and stable across the range of applied stresses, indicating that the fracture network maintains good flow pathways under these conditions. As temperature increases, conductivity tends to decrease, reflecting the influence of thermal effects on the fracture structure. While axial stress also affects conductivity, with higher stresses generally leading to reduced flow due to pore closure, the dominant factor appears to be temperature. At elevated temperatures, conductivity is generally lower across the range of stresses, suggesting that thermal effects increasingly influence fracture performance. Overall, the data indicates a consistent negative correlation between temperature and conductivity, with axial stress providing an additional, secondary influence on flow behavior.

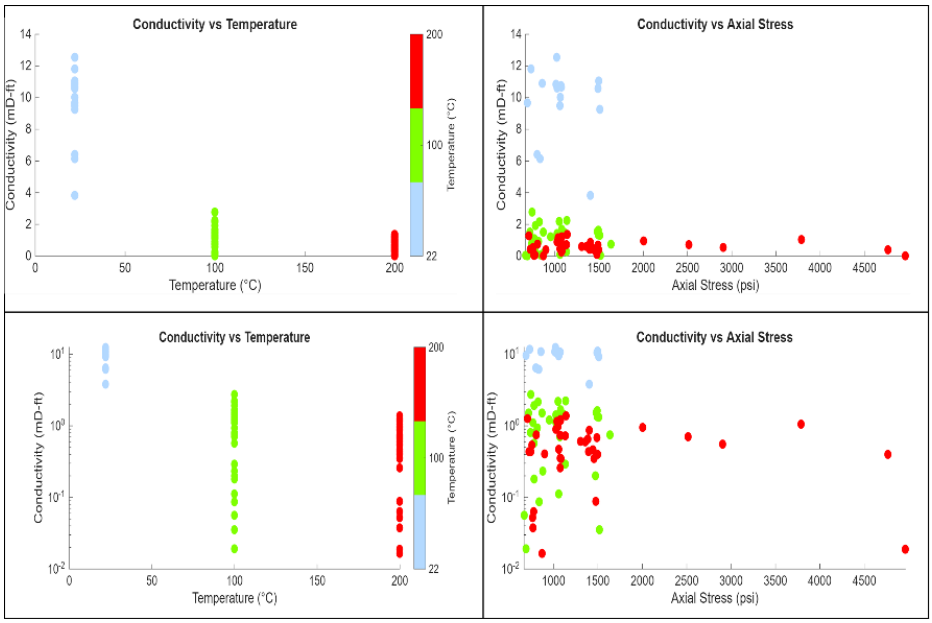

Figure 11. PC proppant test results (Color denotes temperature, increasing from low (cool colors) to high (warm colors)). Left column: Proppant pack conductivity as a function of temperature, showing a consistent decrease as temperature increases from 22 °C to 200 °C. Right column: Conductivity response to axial stress as temperature increases from 22 °C to 200 °C, illustrating that higher temperatures accelerate conductivity loss under increasing stress. Upper row: Conductivity plotted on a linear y-axis. Lower row: Same data plotted on a logarithmic y-axis to highlight order-of-magnitude changes at low conductivity levels.

At room temperature and under low to intermediate stress conditions, all proppant beds exhibit high conductivity. Conductivity values above ~1 mD-ft in our system indicate that the sample is highly permeable and effectively "transparent" to flow. Conductivity can vary even under similar stress and temperature conditions, reflecting sensitivity to the loading path and the applied pressure gradient. To better

approximate field conditions, we impose a pressure gradient of a few psi across the sample length (several centimeters) while maintaining a mean fluid pressure of ~1000 psi, consistent with typical injection-well conditions. When scaled to reservoir dimensions, this corresponds to several hundred psi of pressure drop over 10–100 m. However, when conductivity becomes too low, the injection pressure must be increased to maintain a consistent flow regime and ensure stable measurements. As axial stress increases, conductivity generally decreases, although the trend is not strictly monotonic. Elevated temperatures also lead to a reduction in conductivity.

5.4 Sample ReE (Sand):

During conductivity testing of sand, the axial load was cycled below 6500 psi while the temperature was elevated to a maximum of 220 ℃. Throughout the experiment, fluid effluent was collected at each temperature stage to monitor changes. A slight darkening of the effluent was observed as temperature increased, shifting from initially clear to a darker hue (Figure 12, left). This change suggests potential thermal degradation of the sand, mobilization of fines, or dissolution products. Sand color was initially bright reddish yellow before testing, whereas post-test observations showed a clear loss of color intensity. During the conductivity tests conducted using sand proppant, several operational challenges were encountered. As the axial load and temperature were progressively increased, significant fine generation was observed, which led to partial blockage of the flow lines and hindered stable fluid circulation through the system. Repeated flow-line blockage required intermittent shutdowns and cleaning of the system. These interruptions became more frequent at higher axial loads and temperatures; as such, conductivity data beyond 4000 psi may be subject to increased uncertainty. Post-test inspection showed that the sand bed remained unconsolidated, with approximately 54% fines generated after a 10-minute sieve analysis. At stresses exceeding the packing strength, the generation of fines may have promoted more complicated flow paths within the proppant bed. Consequently, the conductivity measurements at higher pressures might require further verification.

Figure 12: Left: Effluent fluid across temperature stages during Sand proppant testing. Right: The sand Bed after exposure to final conditions of 6,000 psi (which exceeds crush resistance ~910psi of the sand) and 200 °C.

SEM analysis captures temperature- and stress-induced microstructural changes beyond macroscopic observation. SEM images of Sand 10/35 proppant were collected at multiple magnifications to capture both compositional contrast and surface morphology (Figure 13) Panels (a), (b), and (c) show no discernible color contrast, indicating the absence of foreign materials within the sand bed. Panels (e), (D), and (F) illustrate the corresponding surface morphology, revealing pronounced microstructural alteration. Clear evidence of fine generation and microcracks is observed, reflecting the combined influence of elevated temperature and mechanical loading. These microstructural changes reduce intergranular pore space and represent a key mechanism contributing to the observed decline in fracture conductivity.

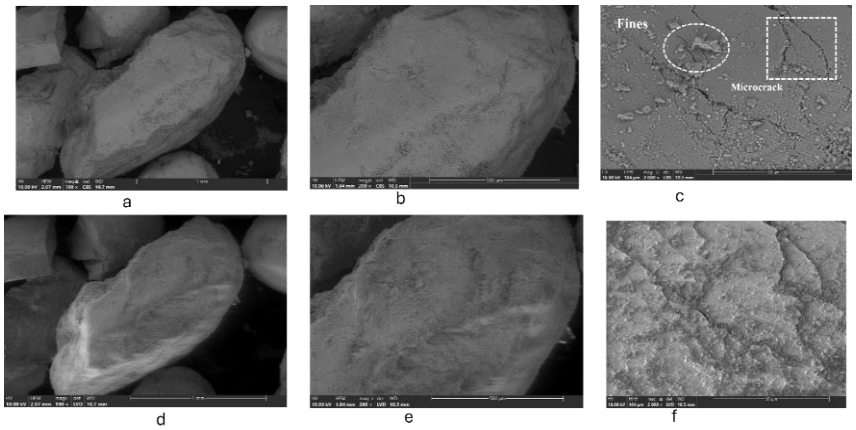

Fig 13: SEM micrographs of Sand 10/35 proppant after combined thermal and mechanical loading. Panels (a–c) present compositional contrast at 50×, 200×, and 2000× magnification, highlighting bright regions associated with foreign material or thermally affected resin. Panels (d–f) show corresponding surface-morphology views, revealing pronounced microstructural modification. Features such as fine materials, and microcracks are evident, indicating progressive degradation of grains and narrowing of pore pathways by the fines under elevated temperature and stress.

In this experiment, a modified thermal loading path was applied to investigate the potential for conductivity recovery. Instead of sequential heating, the temperature increased directly from 22 °C to 220 °C, followed by stepwise cooling to 100 °C and 50 °C, and subsequent reheating to 180 °C. The results indicate that fracture conductivity is strongly dependent on both temperature and axial stress. At an axial stress of approximately 1000 psi, conductivity at 22 °C is substantially higher than that measured at elevated temperatures.
Following direct exposure to 220 °C, conductivity decreased significantly and exhibited only minor variation with further increases in axial stress, fluctuating around ~1 md-ft. Although conductivity values at 220 °C appear relatively stable compared to subsequent lower-temperature stages, reducing the temperature did not result in conductivity recovery. Conductivity measured at 100 °C, 50 °C, and during reheating to 180 °C remained consistently lower than the initial room-temperature values. This behavior suggests that early exposure to high temperatures induces irreversible damage within the confined sand pack. The combined effects of elevated temperature and increasing axial stress likely enhance grain-to-grain contact stresses, promote grain crushing and fines generation, and lead to permanent flow-path blockage. The absence of recovery during cooling and reheating indicates that the system stabilizes in a mechanically damaged state, demonstrating strong dependence on thermal loading history rather than reversible thermal effects.

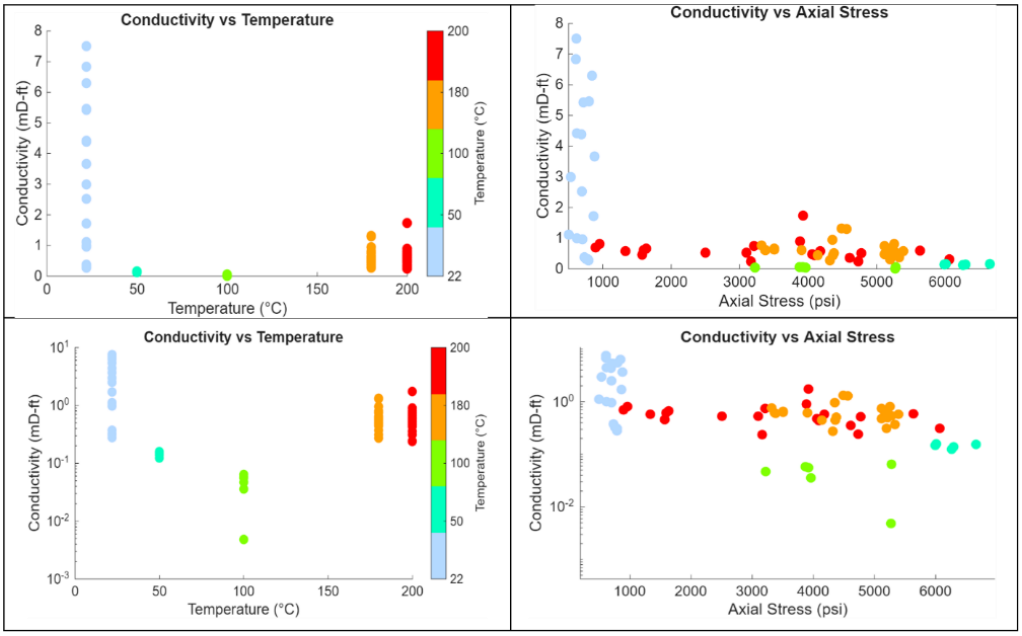

Fig. 14. Sand proppant test results (Color denotes temperature, increasing from low (cool colors) to high (warm colors)). Left column: Proppant pack conductivity as a function of temperature, showing conductivity decrease with increasing temperature. Right column: Conductivity response to axial stress as temperature increases from 22 °C to 200 °C, illustrating that higher temperatures accelerate conductivity loss under increasing stress. Upper row: Conductivity plotted on a linear y-axis. Lower row: Same data plotted on a logarithmic y-axis to highlight order-of-magnitude changes at low conductivity levels. As the axial load and temperature were progressively increased, significant fine generation was observed, which led to partial blockage of the flow lines and hindered stable fluid circulation through the system. Repeated flow-line blockage required intermittent shutdowns and cleaning of the system. These interruptions became more frequent at higher axial loads and temperatures; as such, conductivity data beyond 4000 psi may be subject to increased uncertainty.

CONCLUSIONS

This study investigated the high-temperature, high-pressure performance of low-density ceramics (LDC), resin-coated ceramics (RC), and petroleum coke (PC) and sand under conditions representative of deep geothermal reservoirs. Fracture conductivity was measured over a range of axial stresses and temperatures, complemented by SEM analysis to assess pre- and post-test microstructural changes. LDC consistently exhibited the highest conductivity, followed by RC, while PC and Sand showed the poorest performance. Conductivity decreased markedly with increasing temperature and stress and was largely irreversible. Variations in stress path and pressure gradient further influenced conductivity, underscoring the roles of loading history and flow conditions. Overall, fracture conductivity was controlled by the combined effects of packing strength, effective stress, temperature, pore pressure, and flow rate under extreme conditions.

SEM observations showed that PC suffered severe grain breakage, LDC experienced moderate cracking and partial fusion, and RC largely retained intact grain morphology. Sand exhibited significant fines generation and surface damage. These microstructural changes align with conductivity loss, indicating that grain integrity governs fracture flow performance under high-temperature conditions.

At temperatures above ~220 °C, the proppants exhibited markedly different conductivity responses. LDC showed high initial conductivity but suffered a sharp, irreversible decline with increasing stress, approaching zero near ~250 °C due to melting of the sealing material and flow blockage. RC and PC maintained conductivity at moderate stress but experienced significant, non-recoverable reductions at elevated

stress and temperature due to thermally induced grain damage. In contrast, sand failed rapidly upon heating, with extensive fines generation and unstable flow, indicating poor suitability for high-temperature fracture applications.

Overall, the results underscore the importance of proppant selection for maintaining long-term fracture conductivity in harsh reservoir environments. The choice of material must account for coupled thermal, mechanical, and microstructural effects to ensure sustained reservoir productivity.

ACKNOWLEDGEMENT:

The authors sincerely appreciate the support provided by the OU Reservoir Geomechanics and Seismicity Group. The authors would like to thank lab manager Steve and Dr. Peter Larson from Samuel Roberts Noble Microscopy Laboratory, OU, for their invaluable assistance on SEM. The authors also would like to thank 'Carbo Ceramic' for providing necessary proppants to conduct this research. This project was supported by the Utah FORGE project sponsored by the U.S. Department of Energy, through the project 'Development and testing of tagged proppant for fracture conductivity enhancement and reservoir characterization in EGS'.

REFERENCES

Ye, Z., & Ghassemi, A. (2018). Injection-Induced Shear Slip and Permeability Enhancement in Granite Fractures. *Journal of Geophysical Research: Solid Earth*, *123*(10), 9009–9032. https://doi.org/10.1029/2018JB016045

Cooke, C. E., 1973. *Conductivity of Fracture Proppants in Multiple Layers*. http://onepetro.org/JPT/article-pdf/25/09/1101/2225477/spe-4117-pa.pdf/1

Duenckel, R., Moore, N., O'Connell, L., Abney, K., Drylie, S., & Chen, F. (2016). *The Science of Proppant Conductivity Testing — Lessons Learned and Best Practices.* SPE Hydraulic Fracturing Technology Conference (paper SPE-179125-MS).

Hu, X., Wu, K., Li, G., Tang, J., & Shen, Z. (2018). Effect of proppant addition schedule on the proppant distribution in a straight fracture for slickwater treatment. *Journal of Petroleum Science and Engineering*, *167*, 110–119. https://doi.org/10.1016/J.PETROL.2018.03.081.

Ko, S., Ghassemi, A., Uddenberg, M. 2023. *Selection and Testing of Proppants for EGS*. PROCEEDINGS, 48 th Workshop on Geothermal Reservoir Engineering Stanford University, Stanford, California, February 6-8, 2023, SGP-TR-224

Kurz, B., Schmidt, D., & Cortese, P. (2013). *SPE 163849 Investigation of Improved Conductivity and Proppant Applications in the Bakken Formation*. http://onepetro.org/SPEHFTC/proceedings-pdf/13HFTC/13HFTC/D011S002R008/1574152/spe-163849-ms.pdf/1

Liang, T., Zhou, F., Shi, Y., Liu, X., Wang, R., Li, B., & Li, X. (2018). Evaluation and optimization of degradable-fiber-assisted slurry for fracturing thick and tight formation with high stress. *Journal of Petroleum Science and Engineering*, *165*, 81–89. https://doi.org/10.1016/J.PETROL.2018.02.010.

Liu, Z., & Reynolds, A. C. (2021). Gradient-enhanced support vector regression for robust life-cycle production optimization with nonlinear-state constraints. *SPE Journal*, *26*(4), 1590–1613. https://doi.org/10.2118/204236-PA

Lopez-Bonetti, E., Cuessy, A., Coronel, H., & Suarez-Fromm, J. D. (2014). *SPE-169316-MS Advanced Technique for Enhancing Fracture Conductivity in Tight-Gas Condensate Reservoirs through Applying Liquid Resins: Case Histories from Burgos Basin, Mexico*. http://onepetro.org/SPELACP/proceedings-pdf/13LACP/13LACP/D031S025R002/3678233/spe-169316-ms.pdf/1

Mattson, E. D., Huang, H., Conway, M., & O'Connell, L., (2014). Discrete Element Modeling Results of Proppant Rearrangement in Cooke Conductivity Cell. SPE 168604, 9.

Merey, Ş. (2019). Prediction of transport properties for the Eastern Mediterranean Sea shallow sediments by pore network modelling. *Journal of Petroleum Science and Engineering*, *176*, 403–420. https://doi.org/10.1016/J.PETROL.2019.01.081.

Moore, J., McLennan, J., Pankow, K., Simmons, S., Podgorney, R., Wannamaker, P., Jones, C., Rickard, W., Xing, P., 2020. The Utah Frontier Observatory for Research in Geothermal Energy (FORGE): A Laboratory for Characterizing, Creating and Sustaining Enhanced Geothermal Systems. Proceedings, 45th Workshop on Geothermal Reservoir Engineering, Stanford University, Stanford, California, February 10-12, 2020. SGP-TR-216.

Nguyen, P., Weaver, J., & Rickman, R. (2008). *SPE 118175 Prevention of Geochemical Scaling in Hydraulically Created Fractures: Laboratory and Field Studies*. http://onepetro.org/SPEERM/proceedings-pdf/08ERM/08ERM/SPE-118175-MS/2740218/spe-118175-ms.pdf/1

Shah, S. N. (2010). *SPE 128612 Fracture Orientation and Proppant Selection for Optimizing Production in Horizontal Wells*. http://onepetro.org/SPEOGIC/proceedings-pdf/10OGIC/10OGIC/SPE-128612-MS/4056753/spe-128612-ms.pdf/1

Suponik, T., Labus, K., & Morga, R. (2023). Assessment of the Suitability of Coke Material for Proppants in the Hydraulic Fracturing of Coals. Materials, 16(11).https://doi.org/10.3390/ma16114083.

Sutradhor, S. S., Ghassemi, A., 2025. Crush Resistance and Packing Strength of Candidate Proppant for Enhanced Geothermal Systems. In PROCEEDINGS, 50th Workshop on Geothermal Reservoir Engineering Stanford University, Stanford, California, February 10-12, 2025 SGP-TR-229.

Zheng, W., Silva, S. C., & Tannant, D. D. (2018). Crushing characteristics of four different proppants and implications for fracture conductivity. Journal of Natural Gas Science and Engineering, 53, 125–138. https://doi.org/10.1016/j.jngse.2018.02.028

Zoveidavianpoor, M., Gharibi, A., & bin Jaafar, M. Z. (2018). Experimental characterization of a new high-strength ultra-lightweight composite proppant derived from renewable resources. *Journal of Petroleum Science and Engineering*, *170*, 1038–1047. https://doi.org/10.1016/J.PETROL.2018.06.030.